NANO LETTERS

pubs.acs.org/NanoLett Letter

Black Phosphorus Mid-Infrared Light-Emitting Diodes Integrated with Silicon Photonic Waveguides

Tian-Yun Chang, Yueyang Chen, De-In Luo, Jia-Xin Li, Po-Liang Chen, Seokhyeong Lee, Zhuoran Fang, Wei-Qing Li, Ya-Yun Zhang, Mo Li, Arka Majumdar,* and Chang-Hua Liu*

Cite This: https://dx.doi.org/10.1021/acs.nanolett.0c02818 Read Online

ACCESS | Metrics & More | Article Recommendations | Supporting Information

ABSTRACT: Light-emitting diodes (LEDs) based on III−V/II−VI materials have delivered a compelling performance in the mid-infrared (mid-IR) region, which enabled wide-ranging applications in sensing, including environmental monitoring, defense, and medical diagnostics. Continued efforts are underway to realize on-chip sensors via heterogeneous integration of mid-IR emitters on a silicon photonic chip, but the uptake of such an approach is limited by the high costs and interfacial strains, associated with the processes of heterogeneous integrations. Here, the black phosphorus (BP)-based van der Waals (vdW) heterostructures are exploited as room-temperature LEDs. The demonstrated devices emit linearly polarized light, and the spectra cover the technologically important mid-IR atmospheric window. Additionally, the BP LEDs exhibit fast modulation speed and exceptional operation stability. The measured peak extrinsic quantum efficiency is comparable to the III−V/II−VI mid-IR LEDs. By leveraging the integrability of vdW heterostructures, we further demonstrate a silicon photonic waveguide-integrated BP LED.

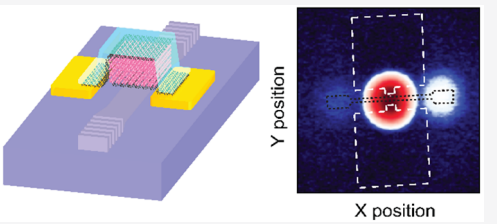

KEYWORDS: *electroluminescence, van der Waals heterostructures, black phosphorus, mid-infrared, optoelectronics, silicon photonics*

The development of light sources compatible with a silicon platform is essential for silicon photonic technologies. Hybrid integration of III−V/II−VI semiconductors for on-chip light sources has long been pursued, and multiple research works have successfully demonstrated that their spectral coverage can extend from the near-IR to mid-IR region.[1−3] Such capabilities have expanded the applications of silicon photonics from traditional telecommunications to lab-on-chip spectroscopic sensing, as many chemical species have strong absorption fingerprints in the mid-IR band.[4−6] Despite continued advancements, the current on-chip sources are still realized via wafer bonding or direct heteroepitaxial growth of III−V/II−VI on the silicon chip. Such an approach necessarily results in increased fabrication costs and complex device structures. Furthermore, these heterogeneous integration processes cause the interfacial strains, originated from the lattice- and thermal-mismatch, and consequently, lead to luminescence quenching of on-chip emitters.[4−6]

To that end, van der Waals (vdW) materials have recently emerged as a promising alternative approach. One of the key reasons is that vdW materials cover a wide range of optical band gaps, offering the opportunities of developing vdW-based optoelectronics at different spectral regions.[7−9] Additionally, due to the weak vdW bonding of these materials, different vdW materials can be vertically stacked to form heterostructures. Further, these materials and their heterostructures can be integrated onto integrated photonic structures, such as cavities or waveguides, just via transfer, without stringent requirement on lattice matching.[10−15] So far, diverse vdW-based LEDs, exploiting transition metal dichalcogenides (TMDs) as the emissive layers, have been integrated with photonics and performed in the visible to near-IR region.[7,9,11,12,15] The mid-IR vdW LEDs have been realized very recently using BP/TMDs heterostructures,[16,17] but their integrations with mid-IR on-chip photonics remain experimentally unexplored. In this Letter, we present a LED simply composed of two graphite contacts sandwiching a BP flake. Under a bias voltage, the high density of current could be stably injected from graphite into BP that leads to linearly polarized mid-IR light emission, associated with the direct narrow gap (∼0.3 eV) and anisotropic optoelectronic properties of BP.[18−22] By integrating the vdW heterostructures with an on-chip silicon waveguide, we further demonstrate that the emission of BP-based LED can evanescently couple and propagate through the waveguide, showing its potential applications in on-chip mid-IR light sources.

Figure 1a,b shows the optical micrograph and schematic of the hBN-encapsulated LED, composed of the 87 nm thick BP sandwiched by two graphite electrodes (see Methods). The

Received: July 9, 2020
Revised: August 20, 2020
Published: August 20, 2020

https://dx.doi.org/10.1021/acs.nanolett.0c02818
Nano Lett. XXXX, XXX, XXX−XXX

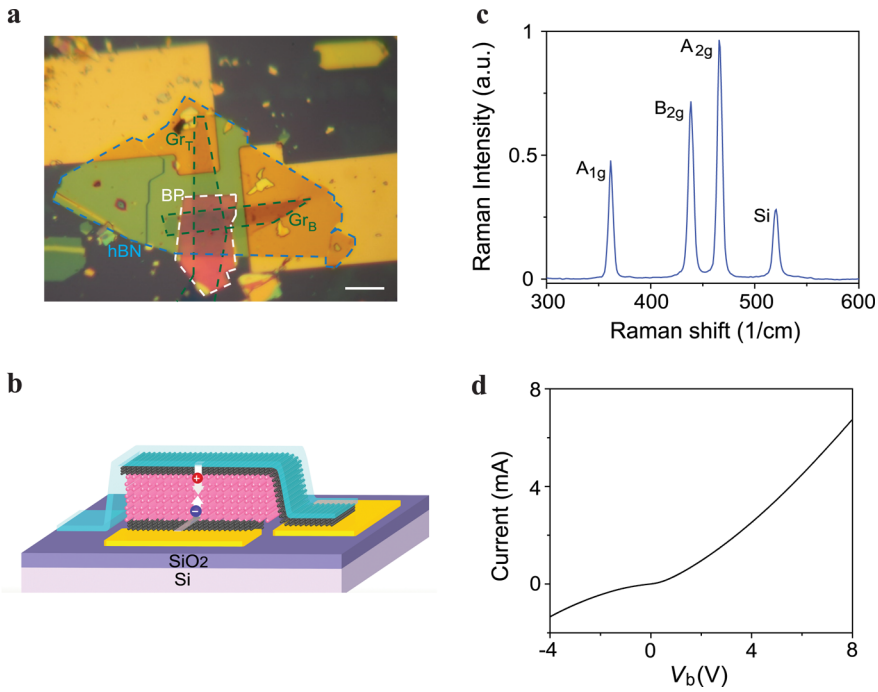

Figure 1. BP-based vdW heterostructures. (a) Optical microscope image of the BP-based vdW heterostructures. The regions of Gr, BP, and hBN are defined by green, white, and blue dashed lines, respectively. Scale bar, 20 μm. (b) Schematic of the device configuration, composed of vertically stacked hBN/Gr_T/BP/Gr_B heterostructures. The injected electrons and holes from two Gr contacts would recombine in the BP flake, leading to electroluminescence. (c) Raman spectrum of the used BP flake, showing three characteristic Raman peaks. The spectrum was collected with λ = 532 nm excitation. (d) $I-V$ characteristic of the BP-based heterostructures.

bulk BP, used here as the light-emitting layer, exhibits three characteristic Raman peaks (Figure 1c). The top (Gr_T) and bottom (Gr_B) graphite electrodes are semitransparent in the mid-IR region[23] and capable of injecting a high density of current into BP. To probe the basic electronic properties of heterostructures, the bias voltage (V_b) was applied across two graphite contacts with the Gr_T being grounded. As shown in Figure 1d, the device exhibits nonlinear and asymmetric $I-V$ characteristics, which reflects the dissimilarities of two Schottky barriers at BP/Gr interfaces.[24] The detailed information on the band bending of two barriers can be resolved using the scanning photocurrent microscopy (Figure S1). In addition, it is notable that the graphite contacts can inject up to 6.7 mA current into ~1200 μm^2 BP flake. Such a high current density (5.58×10^5 mA/cm^2) injection could potentially lead to the detectable electroluminescence signal.

We built the experimental setup as schematically illustrated in Figure 2a (also see Methods) to characterize the luminescence of vdW heterostructures. As an initial experiment, the bias voltage (V_b = 6 V) was applied to the LED, mounted on the $x-y$ scanning stage. The generated electroluminescence signal was mechanically chopped and detected by a liquid-nitrogen-cooled indium antimonide (InSb) detector and lock-in amplifier (Figure 2a, green beam path). This allows us to resolve the spatial distribution of electroluminescence (Figure 2b). To gain further insight, we also conducted the scanning reflection experiment, which is helpful in identifying the position of the objective focal point on the measured device. The excitation wavelength is selected at 3.5 μm, as BP is highly absorbing in this spectral region, leading to a better reflectivity contrast of the image (Figure 2c). By comparing these two scanning images, it is clear that the emission originates from the heterostructures and its peaks from the region, where Gr_T and Gr_B are overlapped with each other.

We next analyzed the spectral characteristic of the BP emitter via sending the electroluminescence signals to a monochromator, as shown in the red beam path in Figure 2a (see Methods). Figure 2d presents the electroluminescence spectra for different bias voltage V_b. The results show that all spectra have the same peak wavelength ~3.64 μm, which is also in good agreement with our photoluminescence measurement of the BP (Figure 2e).[25] Such a feature indicates that the measured electroluminescence is originated from the recombination of electrons and holes, injected from graphite contacts, rather than the thermal blackbody radiation, as the peak wavelength is close to the band gap of bulk BP. However, we note that the spectral width of electroluminescence at V_b = 1 V is ~0.585 μm (calculated by measuring the full width at half-maximum, fwhm), which is wider than the line width of photoluminescence (fwhm ~0.423 μm). In addition, when the V_b is changed to 8 V, the fwhm of electroluminescence increases to ~0.65 μm. This observed spectral broadening suggests that the large vertical field (as high as 0.9 MV/cm at V_b = 8 V) and high current injection density could redistribute the carriers into higher energy states in the momentum space of BP. Similar effect was reported for the TMD-based emitter in the past.[26]

After characterizing the emission spectrum, we calibrated the output power of the BP mid-IR LED, operated at various bias voltages (Figure S2). The results shown in Figure 2f reveal that bipolar charge injection into the emissive BP layer can occur at a very low bias voltage (V_b ~ 0.45 V). The BP with light-emitting area ~1200 μm^2 can produce output power approaching 1.8 μW and can also exhibit excellent operation stability over the periods of at least 100 h (see Figure S3).

https://dx.doi.org/10.1021/acs.nanolett.0c02818
Nano Lett. XXXX, XXX, XXX−XXX

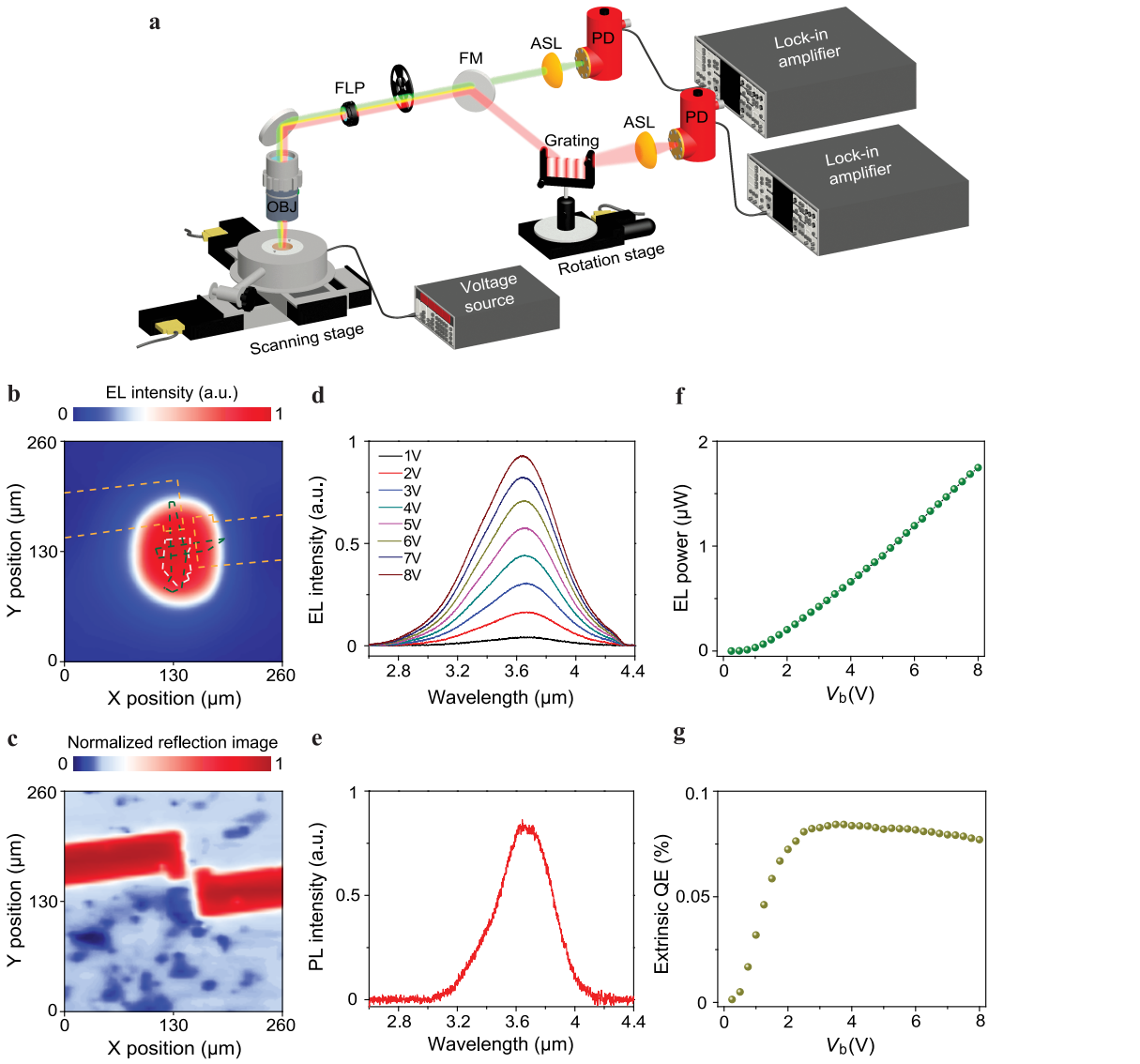

Figure 2. Optoelectronic characterizations of the BP-based vdW heterostructures. (a) Schematic of the experimental setup that can perform the electrical transport, as well as the scanning photocurrent, electroluminescence, and photoluminescence measurements. The green (red) beam path is used to measure the emission power (spectra) of the BP LED. PD, photodetector; FM, flippable mirror; FLP, flippable linear polarizer; ASL, aspheric lens; OBJ, objective (NA = 0.67). (b, c) The spatially resolved two-dimensional (b) electroluminescence map and (c) reflection map. In panel b, the regions of Gr, BP, and metal contacts are defined by green, white, and orange dashed lines, respectively. The results were obtained, as the device shown in Figure 1a was biased at 6 V. (d) Bias dependence of electroluminescence spectra, emitted by the BP LED. (e) Photoluminescence spectrum measured from the used BP flake. The excitation wavelength is 2.5 μm, and excitation power is 500 μW. (f) Device emission powers at various bias voltages. (g) Extrinsic QE of the BP LED, operated at various bias voltages.

These features highlight the usefulness of our BP LED for practical applications. The extrinsic QE (η) of our BP LED can be quantified by[10]

$$\eta = \frac{qN}{I}$$

where q is the electron charge, N the number of photons emitted into the free space per second, and I the current injected into BP LED (see Supporting Information for the calculation). As shown in Figure 2g, the extrinsic QE can reach 0.084% at V_b = 3.5 V. This performance is comparable to other III−V mid-IR LEDs.[2,27] By further increasing the bias voltage to 8 V, the efficiency only slightly decreases to 0.077%, showing the small reduction of efficiency with increasing current. Notably, the low-efficiency droop performance can be observed in multiple BP LEDs we fabricated (Figure S4). This indicates BP could be a promising light-emitting material, likely owning to its negligible Auger process.[28,29]

To investigate the polarization properties of the BP emitter, a linear polarizer was added in the light collection path (green beam path, Figure 2a). Figure 3a presents a color map of the polarization angle-dependent photoluminescence amplitude of BP, as a function of excitation power (λ = 2.5 μm). The calculated degree of polarization factors (ρ) is ~80% (Figure 3b), associated with the property of anisotropic optical transition near the band edge of BP,[18−20,24,25] and the measured factors are less than unity, suggesting the momentum distribution of photoexcited carriers in BP could be affected by the scattering processes. For comparison, we also characterized the emission anisotropy of electroluminescence of the BP LED,

https://dx.doi.org/10.1021/acs.nanolett.0c02818
Nano Lett. XXXX, XXX, XXX−XXX

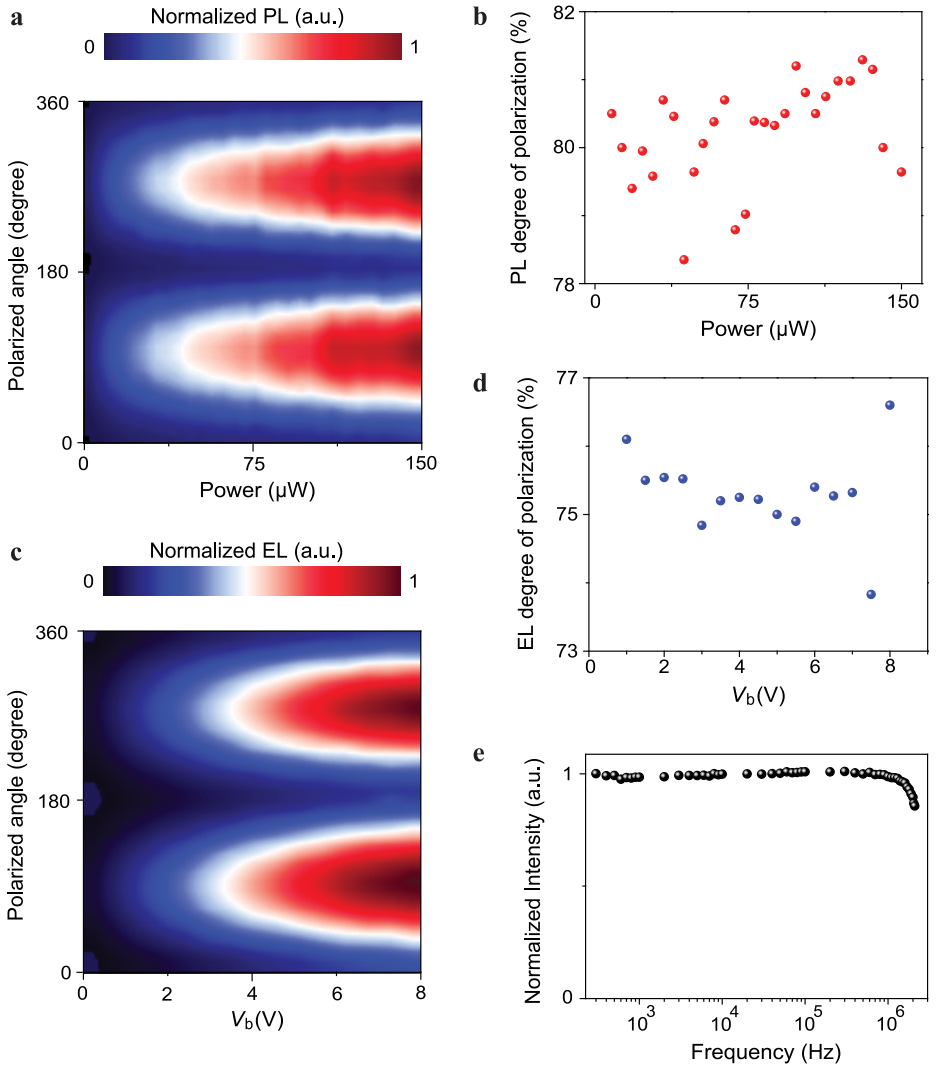

Figure 3. Polarization-resolved and frequency-dependent electroluminescence. (a) Linear polarization-dependent mapping of BP photoluminescence intensity (I_{PL}) under various excitation powers (λ = 2.5 μm). (b) Power-dependent degree of polarization of photoluminescence, which is quantified by the formula $\frac{I_{PL,max} - I_{PL,min}}{I_{PL,max} + I_{PL,min}}$. The calculations are based on the results shown in panel a. (c) Linear polarization-dependent mapping of BP electroluminescence intensity (I_{EL}) under various bias voltages. (d) Bias-dependent degree of polarization of electroluminescence, which is quantified by the formula $\frac{I_{EL,max} - I_{EL,min}}{I_{EL,max} + I_{EL,min}}$. The calculations are based on the results shown in panel c. (e) Frequency response of the BP LED. For this experiment, voltage pulses generated from a function generator not only modulated the electroluminescence of BP LED but also served as a reference signal of the lock-in amplifier. The modulated electroluminescence signal passed along the green beam path was shown in Figure 2a and was then detected by the InAsSb detector and lock-in amplifier. By tuning the on−off frequency of voltage pulses, the variation of photovoltage measured by the lock-in amplifier was recorded. The measured photovoltage is normalized with respect to the peak intensity.

under different bias voltages (Figure 3c). The measured electroluminescence amplitude shows the same polarization angle-dependent variations. The calculated polarization factors of electroluminescence (Figure 3d) are close to the photoluminescence results, indicating the possibility of applying BP LEDs as highly polarized mid-IR sources.

Next, we characterized the frequency response of the BP LED via electrically turning it on and off at different modulation frequencies and monitoring the change of photovoltages, detected by the lock-in amplifier. For this experiment, the detector used to collect electroluminescence signals (Figure 2a, green beam path) was replaced with a room-temperature indium arsenide antimonide (InAsSb) detector due to its faster operation speed (9 MHz bandwidth, Thorlabs PDA07P2). We note that, while the InAsSb detector has a mediocre photoresponsivity (~4 mA/W), the frequency dependence of electroluminescence can still be successfully resolved (Figure 3e). We measured the 3 dB roll-off frequency as ~2 MHz, limited by the bandwidth of the lock-in amplifier. These demonstrations clearly show the opportunities of using the reported BP LED for free space sensing or spectroscopic applications without the need of external modulators.

Finally, we explored the potential of using our BP heterostructure LEDs for mid-IR-integrated silicon photonics. Figure 4a,b shows the scanning electron micrograph (SEM) and schematic of the hybrid device: the BP LED is integrated onto a mid-IR silicon waveguide with two grating couplers at both ends. The details of the design, fabrication, and simulation are described in Methods and Supporting Information. When applying the bias voltage across two

https://dx.doi.org/10.1021/acs.nanolett.0c02818
Nano Lett. XXXX, XXX, XXX−XXX

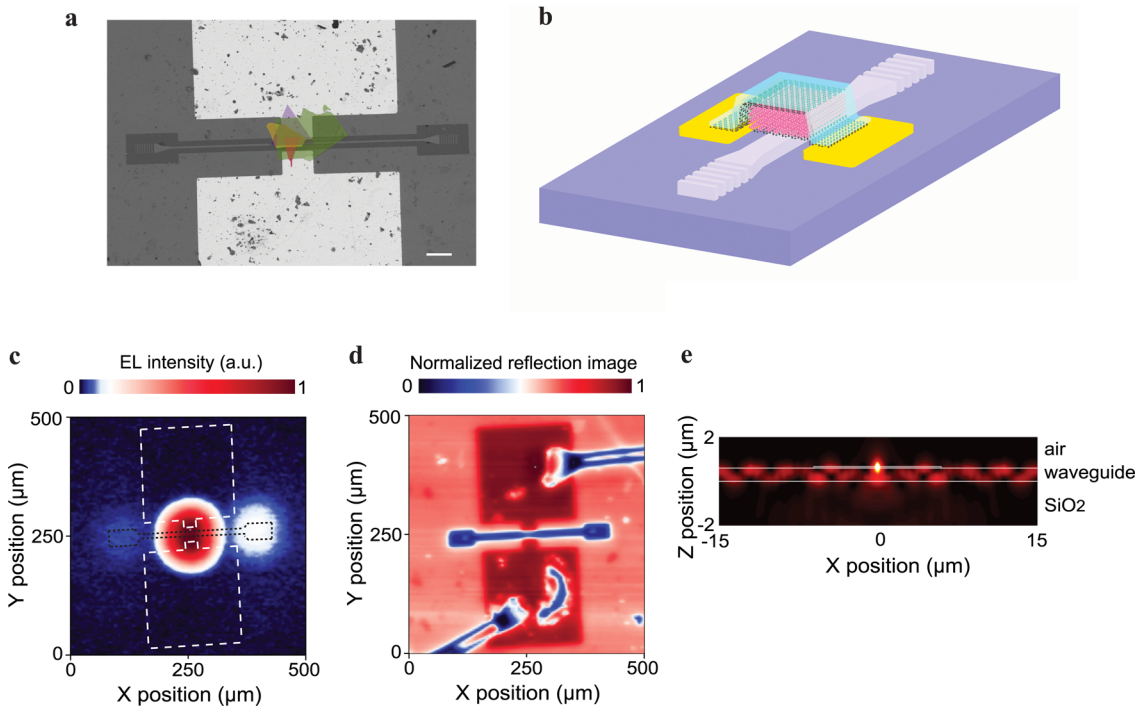

Figure 4. The waveguide-integrated BP LED. (a) A false-color SEM image of the waveguide-integrated BP LED. The emitter is composed of the vertically stacked hBN (green)/Gr_T (red)/BP (yellow)/Gr_B (purple) heterostructures. The used BP flake is 65 nm thick. Scale bar, 50 μm. (b) Schematic of the hBN-encapsulated BP LED on top of a silicon waveguide. (c, d) The spatially resolved two-dimensional (c) electroluminescence map, and (d) reflection map (illumination wavelength: 3.5 μm). The electroluminescence results were obtained, and the device shown in panel a was biased at 3 V. In panel c, the regions of metal electrodes are outlined with white dashed lines, and the regions of waveguide and grating couplers are outlined with black dashed lines. (e) An FDTD simulation of the cross-section of the electric field intensity distribution. In this simulation, a BP flake is placed on top and at the center of a 600 nm-thick silicon waveguide, and there is a 2 μm thick silicon oxide layer beneath the silicon waveguide. The thickness and lateral size of BP flake are set to 65 nm and 50 μm, respectively. The refractive index of BP is assumed to be (n,k) = (4.4,0.2).[33] A dipole source with orientation along the y-axis is placed at the center of the BP layer.

graphite contacts, three bright spots can be observed from the scanning electroluminescence map (Figure 4c), distinct from the scanning result shown in Figure 2b. Moreover, by comparing the scanning electroluminescence with the reflection maps (Figure 4d), it is clear the central brighter spot corresponds to the position of BP LED, while the two extra emission spots are located at the grating couplers. These evidently confirm that the mid-IR electroluminescence of the BP LED can be evanescently coupled to the silicon photonic waveguide. The coupled light then propagates through the waveguide to the coupler, which redirects the light out to the free space. We note that the coupling of BP emission into the silicon waveguide can also be validated via three-dimensional finite-difference time-domain (FDTD) simulations (Figure 4e). However, the measured emission intensity from the right (left) grating coupler is 10% (6%) with respect to the central BP emissive region, which is lower than the simulation result (40%, see Supporting Information for the calculation and Figure S5). This suggests that the performance of our waveguide-integrated BP LED can be further improved by optimizing the silicon photonics fabrications and minimizing the residue remaining on the waveguide due to the transfer of vdW heterostructures. Additionally, we used a traditional silicon waveguide to demonstrate the coupling in this Letter, and the waveguide designs can be further optimized to increase the coupling efficiency.

In summary, we report a new approach to realize room-temperature mid-IR LEDs that exhibit an exceptional linear degree of polarization, long-term stability, high extrinsic QE, and fast modulation speed. Further engineering of the reported heterostructures will open up new technological opportunities. For example, the emission wavelength could be tuned via applying the mechanical strain or displacement field on the BP heterostructures,[30,31] and emission bandwidth could be expanded into multiple spectral regions by implementing different band gaps of vdW materials into the BP-based heterostructures.[7,8] The efficiency of LED could be higher by improving the quality of the BP flake or enhancing the ambipolar charge injection, realized by asymmetrically controlling the doping of two graphite contacts. Furthermore, we demonstrate the possibility of coupling the emission of BP LED with a silicon waveguide, and the higher coupling efficiency could be realized by utilizing the more advanced photonic structures, such as slot waveguides or photonic crystal waveguides.[12] Considering the recent advancements in the scalable synthesis of vdW materials,[32] we expect that the BP LEDs can be potentially integrated into large-scale photonic integrated circuits, offering tremendous opportunities for mid-IR silicon photonics applications.

METHODS

Fabrication of BP LEDs. The vdW materials present in this work were all prepared by using mechanical exfoliation method, and their thicknesses were identified by atomic force microscopy (AFM). To create the vdW heterostructures, a dry transfer technique was utilized to assemble different materials in the vertical direction.[34] The vertically stacked hBN/Gr_T/BP/Gr_B heterostructures were subsequently transferred onto a

https://dx.doi.org/10.1021/acs.nanolett.0c02818
Nano Lett. XXXX, XXX, XXX−XXX

SiO_2 substrate with prepatterned Cr/Au (5/40 nm) metal electrodes, and during this transfer process, the Gr_T and Gr_B were aligned to attach the two separate metal electrodes. The fabricated BP LEDs were then loaded into a vacuum chamber (10^{-4} Torr) to characterize their optoelectronic properties at room temperature.

Measurement of Emission Powers and Spectra of BP. The green beam path shown in Figure 2a was used to measure the emission powers of the BP LED. For this experiment, the bias voltage was applied to two metal electrodes. The emitted electroluminescence was mechanically chopped and focused onto a liquid nitrogen cooled InSb photodetector (Infrared Associates, IS-2.0). The generated photovoltage was then detected by the lock-in amplifier (Stanford Research Systems, SR865). The detected photovoltage can be converted into the optical power by characterizing the photoresponsivity of InSb photodetector (see Supporting Information, Section 2).

To analyze the spectra of electroluminescence, the light emitted by the BP LED was also mechanically chopped and passed through the red beam path shown in Figure 2a, but this beam path has an additional grating mounted on the rotation stage. The relation between the rotated angle and wavelength detected by the InSb detector was calibrated by coupling the laser, generated by a wavelength-tunable mid-IR optical parametric oscillator (OPO), into the red beam path. For the photoluminescence experiments, a laser beam (λ = 2.5 μm) was coupled into the experimental setup to excite the BP flake. The generated photoluminescence passed through a band-pass optical filter to get rid of the excitation beam reflected from the BP flake, and its spectrum was analyzed using the setup along the red beam path, the same as the electroluminescence measurements.

Fabrication of the Waveguide-Integrated BP LED. The silicon waveguide and grating couplers were fabricated on an SOI chip that consists of a 600 nm of crystalline silicon, 2 μm of oxide, and 500 μm silicon substrate. To create these silicon photonics devices, we spun coat ZEP520A resist on the SOI chip and created the patterns using the ebeam lithography (JEOL JBX6300FX). The patterns were then transferred to the silicon using an inductive-coupled plasma etching in SF6/C4F8 chemistry. The ZEP520A resist was then stripped off by piranha solution. After fabricating the waveguides and grating couplers, two metal contacts were further defined by ebeam overlay, following with atomic layer deposition (ALD), ebeam evaporation, and liftoff. The ALD process deposited 10 nm alumina on the silicon, and the ebeam evaporation process deposited Cr/Au (5/50 nm) as metal contacts. To create the waveguide-integrated BP LED, we exploited the dry transfer technique to integrate the hBN/Gr_T/BP/Gr_B heterostructures onto the silicon waveguide, with the Gr_T and Gr_B attached to two separate metal contacts, and the armchair direction of the BP flake is perpendicular to the silicon waveguide. The fabricated hybrid device was performed at room temperature under a vacuum of 10^{-4} Torr.

■ ASSOCIATED CONTENT

Supporting Information

The Supporting Information is available free of charge at https://pubs.acs.org/doi/10.1021/acs.nanolett.0c02818.

Detailed band diagram of BP heterostructures, output power and extrinsic quantum efficiency of the BP LED, stability measurements, efficiency droop measurements, and FDTD simulation of the waveguide-integrated BP LED (PDF)

■ AUTHOR INFORMATION

Corresponding Authors

Arka Majumdar − *Department of Electrical and Computer Engineering and Department of Physics, University of Washington, Seattle, Washington 98195, United States;* orcid.org/0000-0003-0917-590X

Chang-Hua Liu − *Institute of Photonics Technologies and Department of Electrical Engineering, National Tsing Hua University, Hsinchu 30013, Taiwan;* orcid.org/0000-0001-8042-9218

Authors

Tian-Yun Chang − *Institute of Photonics Technologies, National Tsing Hua University, Hsinchu 30013, Taiwan*

Yueyang Chen − *Department of Electrical and Computer Engineering, University of Washington, Seattle, Washington 98195, United States;* orcid.org/0000-0002-4390-550X

De-In Luo − *Institute of Photonics Technologies, National Tsing Hua University, Hsinchu 30013, Taiwan*

Jia-Xin Li − *Institute of Photonics Technologies, National Tsing Hua University, Hsinchu 30013, Taiwan*

Po-Liang Chen − *Institute of Photonics Technologies, National Tsing Hua University, Hsinchu 30013, Taiwan*

Seokhyeong Lee − *Department of Electrical and Computer Engineering, University of Washington, Seattle, Washington 98195, United States*

Zhuoran Fang − *Department of Electrical and Computer Engineering, University of Washington, Seattle, Washington 98195, United States*

Wei-Qing Li − *Institute of Photonics Technologies, National Tsing Hua University, Hsinchu 30013, Taiwan*

Ya-Yun Zhang − *Institute of Photonics Technologies, National Tsing Hua University, Hsinchu 30013, Taiwan*

Mo Li − *Department of Electrical and Computer Engineering and Department of Physics, University of Washington, Seattle, Washington 98195, United States*

Complete contact information is available at: https://pubs.acs.org/10.1021/acs.nanolett.0c02818

Author Contributions

C.-H.L. and A.M. supervised the project. J.-X.L. and W.-Q.L. exfoliated and characterized the vdW materials. D.-I.L. and Y.-Y.Z. fabricated the vdW heterostructures. Y.C. fabricated the silicon photonics, assisted by S.L., Z.F., and M.L. T.-Y.C. performed the measurements, assisted by P.-L.C. and C.-H.L. All authors contributed to the discussion of the data in the manuscript and Supporting Information.

Notes

During the preparation of this Letter, we became aware of two similar studies, which utilized BP/TMDs heterostructures to create mid-IR LEDs.[16,17]

The authors declare no competing financial interest.

■ ACKNOWLEDGMENTS

The authors thank Prof. Chen-Bin Huang for sharing electronic instruments. This work was supported by the National Tsing Hua University under grant 109Q2715E1, the Ministry of Science and Technology of Taiwan under grant 107-2112-M-007-002-MY3, NSF-1845009, and NSF-ECCS-

https://dx.doi.org/10.1021/acs.nanolett.0c02818
Nano Lett. XXXX, XXX, XXX−XXX

1708579. A.M. also acknowledges support from the Sloan Foundation.

REFERENCES

(1) Biefeld, R. M.; Allerman, A. A.; Kurtz, S. R. Recent advances in mid-infrared (3−6 μ m) emitters. *Mater. Sci. Eng., B* **1998**, *51*, 1−8.
(2) Jung, D.; Bank, S.; Lee, M. L.; Wasserman, D. Next-generation mid-infrared sources. *J. Opt.* **2017**, *19*, 123001.
(3) Kier, A. *Mid infrared semiconductor optoelectronics*; Springer-Verlag: New York, NY, 2006.
(4) Soref, R. Mid-infrared photonics in silicon and germanium. *Nat. Photonics* **2010**, *4*, 495−497.
(5) Lin, H. T.; et al. Mid-infrared integrated photonics on silicon: a perspective. *Nanophotonics* **2017**, *7*, 393−420.
(6) Spott, A.; Stanton, E. J.; Volet, N.; Peters, J. D.; Meyer, J. R.; Bowers, J. E. Heterogeneous Integration for Mid-infrared Silicon Photonics. *IEEE J. Sel. Top. Quantum Electron.* **2017**, *23*, 1.
(7) Xia, F. N.; Wang, H.; Xiao, D.; Dubey, M.; Ramasubramaniam, A. Two-dimensional material nanophotonics. *Nat. Photonics* **2014**, *8*, 899−907.
(8) Geim, A. K.; Grigorieva, I. V. Van der Waals heterostructures. *Nature* **2013**, *499*, 419−425.
(9) Novoselov, K. S.; Mishchenko, A.; Carvalho, A.; Castro Neto, A. H. 2D materials and van der Waals heterostructures. *Science* **2016**, *353*, No. aac9439.
(10) Withers, F.; et al. Light-emitting diodes by band-structure engineering in van der Waals heterostructures. *Nat. Mater.* **2015**, *14*, 301−306.
(11) Liu, C. H.; et al. Nanocavity Integrated van der Waals Heterostructure Light-Emitting Tunneling Diode. *Nano Lett.* **2017**, *17*, 200−205.
(12) Bie, Y. Q.; et al. A MoTe2-based light-emitting diode and photodetector for silicon photonic integrated circuits. *Nat. Nanotechnol.* **2017**, *12*, 1124−1129.
(13) Liu, C. H.; Zheng, J. J.; Chen, Y. Y.; Fryett, T.; Majumdar, A. Van der Waals materials integrated nanophotonic devices. *Opt. Mater. Express* **2019**, *9*, 384−399.
(14) Brar, V. W.; Sherrott, M. C.; Jariwala, D. Emerging photonic architectures in two-dimensional opto-electronics. *Chem. Soc. Rev.* **2018**, *47*, 6824−6844.
(15) Pei, J. J.; Yang, J.; Yildirim, T.; Zhang, H.; Lu, Y. R. Many-Body Complexes in 2D Semiconductors. *Adv. Mater.* **2019**, *31*, 1706945.
(16) Wang, J. J.; et al. Mid-infrared Polarized Emission from Black Phosphorus Light-Emitting Diodes. *Nano Lett.* **2020**, *20*, 3651−3655.
(17) Zong, X.; Hu, H.; Ouyang, G.; Wang, J.; Shi, R.; Zhang, L.; Zeng, Q.; Zhu, C.; Chen, S.; Cheng, C.; Wang, B.; Zhang, H.; Liu, Z.; Huang, W.; Wang, T.; Wang, L.; Chen, X. Black phosphorus-based van der Waals heterostructures for mid-infrared light-emission applications. *Light: Sci. Appl.* **2020**, *9*, 114.
(18) Xia, F. N.; Wang, H.; Jia, Y. C. Rediscovering black phosphorus as an anisotropic layered material for optoelectronics and electronics. *Nat. Commun.* **2014**, *5*, 4458.
(19) Ling, X.; Wang, H.; Huang, S. X.; Xia, F. N.; Dresselhaus, M. S. The renaissance of black phosphorus. *Proc. Natl. Acad. Sci. U. S. A.* **2015**, *112*, 4523−4530.
(20) Wang, X. M.; Lan, S. F. Optical properties of black phosphorus. *Adv. Opt. Photonics* **2016**, *8*, 618−655.
(21) Guo, S. Y.; et al. 2D V-V Binary Materials: Status and Challenges. *Adv. Mater.* **2019**, *31*, 1902352.
(22) Sang, D. K.; Wang, H. D.; Guo, Z. N.; Xie, N.; Zhang, H. Recent Developments in Stability and Passivation Techniques of Phosphorene toward Next-Generation Device Applications. *Adv. Funct. Mater.* **2019**, *29*, 1903419.
(23) Chang, Y. C.; Liu, C. H.; Liu, C. H.; Zhong, Z. H.; Norris, T. B. Extracting the complex optical conductivity of mono- and bilayer graphene by ellipsometry. *Appl. Phys. Lett.* **2014**, *104*, 261909.
(24) Chang, T. Y.; et al. Ultra-broadband, High Speed and High-Quantum-Efficiency Photodetectors based on Black Phosphorus. *ACS Appl. Mater. Interfaces* **2020**, *12*, 1201−1209.
(25) Chen, C.; et al. Bright Mid-Infrared Photoluminescence from Thin-Film Black Phosphorus. *Nano Lett.* **2019**, *19*, 1488−1493.
(26) Li, D. H.; et al. Electric-field-induced strong enhancement of electroluminescence in multilayer molybdenum disulfide. *Nat. Commun.* **2015**, *6*, 7509.
(27) Delli, E.; Hodgson, P. D.; Repiso, E.; Craig, A. P.; Hayton, J. P.; Lu, Q.; Marshall, A. R. J.; Krier, A.; Carrington, P. J. Heteroepitaxial Integration of Mid-Infrared InAsSb Light Emitting Diodes on Silicon. *IEEE Photonics J.* **2019**, *11*, 1.
(28) Bhaskar, P.; Achtstein, A. W.; Vermeulen, M. J. W.; Siebbeles, L. D. A. Radiatively Dominated Charge Carrier Recombination in Black Phosphorus. *J. Phys. Chem. C* **2016**, *120*, 13836−13842.
(29) Ge, S. F.; et al. Dynamical Evolution of Anisotropic Response in Black Phosphorus under Ultrafast Photoexcitation. *Nano Lett.* **2015**, *15*, 4650−4656.
(30) Fei, R. X.; Yang, L. Strain-Engineering the Anisotropic Electrical Conductance of Few-Layer Black Phosphorus. *Nano Lett.* **2014**, *14*, 2884−2889.
(31) Chen, C.; et al. Widely tunable mid-infrared light emission in thin-film black phosphorus. *Sci. Adv.* **2020**, *6*, No. eaay6134.
(32) Eswaraiah, V.; Zeng, Q. S.; Long, Y.; Liu, Z. Black Phosphorus Nanosheets: Synthesis, Characterization and Applications. *Small* **2016**, *12*, 3480−3502.
(33) Bullock, J.; et al. Polarization-resolved black phosphorus/molybdenum disulfide mid-wave infrared photodiodes with high detectivity at room temperature. *Nat. Photonics* **2018**, *12*, 601−607.
(34) Liu, Y.; Weiss, N. O.; Duan, X.; Cheng, H.-C.; Huang, Y.; Duan, X. Van der Waals heterostructures and devices. *Nature Rev. Mater.* **2016**, *1*, 16042.

https://dx.doi.org/10.1021/acs.nanolett.0c02818
Nano Lett. XXXX, XXX, XXX−XXX